21st Australasian Fluid Mechanics Conference
Adelaide, Australia
10-13 December 2018

Resonance in Natural Convection Flow Subjected to Time-varying Thermal Forcing in an Air-filled Cavity

L. Zhou [1], S. W. Armfield[1], N. Williamson[1], M. P. Kirkpatrick[1] and W. Lin[2]

[1]School of Aerospace, Mechanical and Mechatronic Engineering
The University of Sydney, New South Wales 2006, Australia

[2]College of Science and Engineering
James Cook University, Queensland 4811, Australia

Abstract

Numerical simulations were conducted for natural convection flow in an air-filled cavity subjected to periodic heating and cooling at a forcing frequency f on one sidewall, with all other walls adiabatic. The alternating direction thermal boundary layer, produced by the time-varying thermal forcing, discharges hot fluid to the top and cold fluid to the bottom of the cavity. The flow becomes quasi-steady after the initial development, and maintains a time-varying but stable stratification in the cavity interior. The stratification parameter responds at a dominant frequency of two times the forcing frequency, and the time average and fluctuation amplitude are strongly dependent on the forcing frequency. For high Rayleigh number, at $f \cong 0.125$ a resonant effect is observed with an amplification of the stratification variation at the response frequency of $f_{strat} = 0.25$, and the appearance of super- and sub-harmonic modes. This effect is believed to be a result of the interaction of the forcing mode and the mode one internal wave.

Introduction

Natural convection flows occur in a variety of industrial and environmental settings, such as heat exchangers, building ventilation, crystal growth processes and passive cooling systems of nuclear reactors. A classic model is the flow in a differentially heated cavity, with constant temperature or constant heat flux heating and cooling on opposing sidewalls and the remaining walls adiabatic. The heating produces a rising natural convection boundary layer (NCBL) that discharges into a hot intrusion at the top of the cavity, and the cooling on the opposing wall produces a falling NCBL that discharges into a cold intrusion at the bottom. The temperature in the interior is stratified, and the flow follows a cavity scale circulation in the cavity interior [1, 8, 9, 10].

In most cases investigated, flows with constant heating/cooling have been considered. However, in many applications, the thermal boundary condition changes periodically with time, for example, the diurnal heating and cooling of buildings, and frequently energised electrical devices. Kazmierczak and Chinoda [5] were the first to consider the flow in a square cavity subjected to heating/cooling on opposing sidewalls with the hot wall temperature varying sinusoidally with time. As a result of the time-dependent heating, the flow structure changes periodically after initial development. The variations of the horizontal heat transfer rate, quantified by the Nusselt number at the vertical midline, were found to be strongly dependent on the forcing frequency, though the time-averaged value is only marginally different from that of the isothermal case. Lage and Bejan [7] applied a wide range of frequencies for the same configuration, with one sidewall subjected to a time-varying heat flux boundary condition with a square wave shape, and successfully generated resonance, with maximised Nusselt number at the midline. They believed the resonance frequency was associated with the time for the fluid to circle once around the cavity, but that hypothesis did not agree with the numerical results very well. Inspired by Lage and Bejan [7], Kwak and Hyun [6] obtained resonant flows for various Rayleigh numbers and Prandtl numbers. They found that the internal wave oscillation frequency, which is related to the strength of stratification of the flow, gave a better estimation of the resonance frequency. However, their model failed to predict the variation of resonance frequency with the Rayleigh number and Prandtl number. Similar enhancement of horizontal heat transfer due to resonance is also reported in tall and shallow cavities with various aspect ratios [2] and square cavities inclined at an angle [3, 4].

The flow considered here is that of air in a square cavity with all walls non-slip. The left sidewall is subjected to a sinusoidally varying temperature forcing that alternatively heats and cools the fluid in the cavity, with the other walls adiabatic. A range of forcing frequencies are applied to evaluate the effects on stratification, extending our previous work [12] and examining any resulting resonance.

Numerical method

The square cavity is of height and width H, filled with air ($Pr = 0.7$), with all walls non-slip. The flow is initially stationary everywhere in the interior at an ambient temperature T_0. The left sidewall is subjected to a time-varying sinusoidal temperature forcing $T_w = T_0 + \Delta T \sin(2\pi\omega t)$, with the other walls adiabatic. The flow configuration and the time-varying thermal forcing are shown in figure 1, where U and V are velocities in the X and Y directions.

The governing equations and results are presented below in non-dimensional forms with

$$(x,y) = \frac{(X,Y)}{H},\ (u,v) = \frac{(U,V)}{(\alpha/H)\,Ra^{\frac{1}{2}}}, \tag{1}$$

$$\tau = \frac{\alpha t}{H^2} Ra^{\frac{1}{2}},\ p = \frac{H^2 P}{\rho\alpha^2 Ra},\ \theta = \frac{T - T_0}{\Delta T}, \tag{2}$$

where u and v are the non-dimensional velocities in the x and y directions, p the non-dimensional pressure, θ the non-dimensional temperature, and τ the non-dimensional time. The Rayleigh number and Prandtl number are defined as $Ra = (g\beta\Delta T H^3)/(\nu\alpha)$ and $Pr = \nu/\alpha$, with β the coefficient of thermal expansion, ν the kinematic viscosity, and α the thermal diffusivity.

The flow development is obtained by solving the incompressible two-dimensional Navier-Stokes equations and the temperature transport equation, with the Oberbeck-Boussinesq approxima-

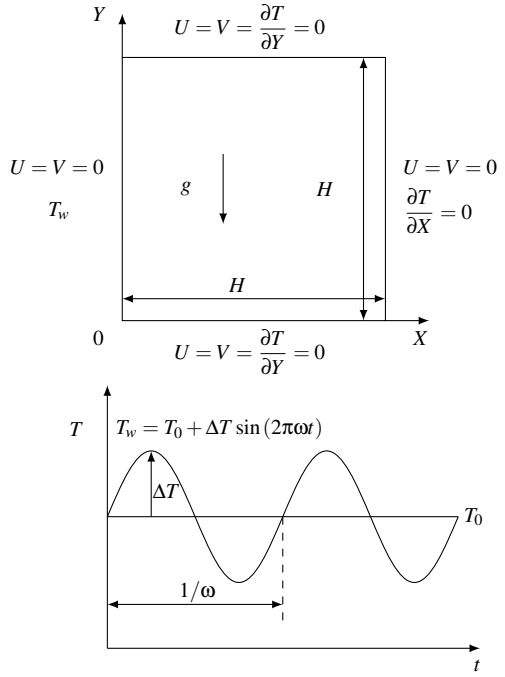

Figure 1: Flow setting and thermal forcing.

tion for buoyancy,

$$\frac{\partial u}{\partial x} + \frac{\partial v}{\partial y} = 0, \tag{3}$$

$$\frac{\partial u}{\partial \tau} + u\frac{\partial u}{\partial x} + v\frac{\partial v}{\partial y} = -\frac{\partial p}{\partial x} + \frac{Pr}{Ra^{\frac{1}{2}}}\left(\frac{\partial^2 u}{\partial x^2} + \frac{\partial^2 u}{\partial y^2}\right), \tag{4}$$

$$\frac{\partial v}{\partial \tau} + u\frac{\partial v}{\partial x} + v\frac{\partial v}{\partial y} = -\frac{\partial p}{\partial y} + \frac{Pr}{Ra^{\frac{1}{2}}}\left(\frac{\partial^2 v}{\partial x^2} + \frac{\partial^2 v}{\partial y^2}\right) + Pr\theta, \tag{5}$$

$$\frac{\partial \theta}{\partial \tau} + u\frac{\partial \theta}{\partial x} + v\frac{\partial \theta}{\partial y} = \frac{1}{Ra^{\frac{1}{2}}}\left(\frac{\partial^2 \theta}{\partial x^2} + \frac{\partial^2 \theta}{\partial y^2}\right). \tag{6}$$

The initial and boundary conditions in the domain $\Omega \in (0,1) \times (0,1)$ in non-dimensional form are

$$x = 0: \; u = v = 0, \; \theta = \sin(2\pi f \tau); \tag{7}$$

$$x = 1: \; u = v = \frac{\partial \theta}{\partial x} = 0; \tag{8}$$

$$y = 0: \; u = v = \frac{\partial \theta}{\partial y} = 0; \tag{9}$$

$$y = 1: \; u = v = \frac{\partial \theta}{\partial y} = 0; \tag{10}$$

$$\tau = 0: \; u = v = \theta = 0. \tag{11}$$

The governing equations are discretised on a non-staggered stretching grid using the finite-difference method. A compact and fourth-order accurate scheme is used for all spatial terms [11]. The time integration uses the second-order Adams-Bashforth and deferred correction Crank-Nicolson methods for the advection and diffusion terms, respectively, with the discrete momentum and temperature equations inverted using a Jacobi solver. Continuity is enforced using the fractional step approach, with the resulting Poisson's equation solved using a Gauss-Seidel method. The grid resolution is 400×400, with the finest cells adjacent to all walls of grid size $\Delta x = 0.0017$ and $\Delta y = 0.0017$, and the coarsest cells in the cavity centre with size 0.0035×0.0035, with a constant expansion ratio of 1.15%. The time-step is $\Delta\tau = 5 \times 10^{-4}$, giving a maximum Courant number of approximately 0.2. To verify the numerical method results have been compared to the transient isothermal case given in Patterson and Armfield [10], and show good agreement with their numerical and experimental data.

Results

After an initial establishment time the fully developed flow achieves a quasi-periodic state. Full development was determined to have been achieved when the moving average and amplitude of the stratification parameter S (defined below) do not vary by more than 0.5% over the last two cycles. Figure 2 contains filled temperature contours for the fully developed flow for $Ra = 1 \times 10^8$, $Pr = 0.7$ and $f = 0.08$, showing the time variation of the flow over a single heating cooling phase.

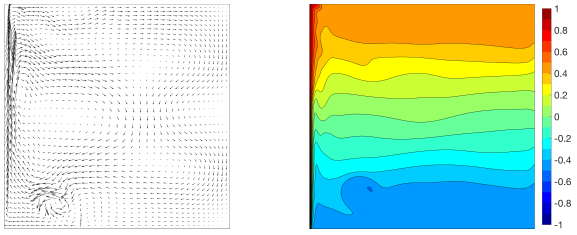

(a) $\tau = 2003.125$ (maximum heating)

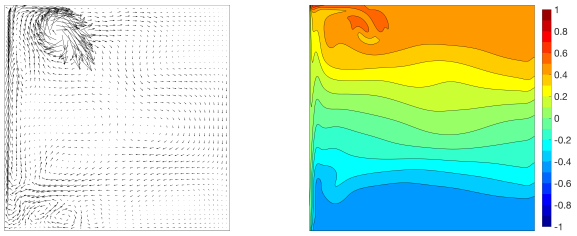

(b) $\tau = 2006.25$ (end of heating)

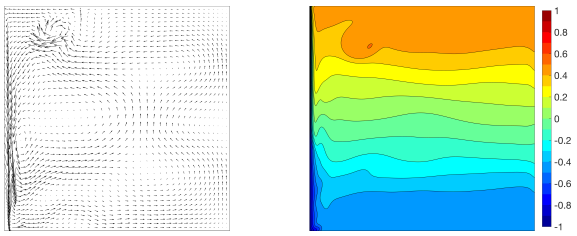

(c) $\tau = 2009.375$ (maximum cooling)

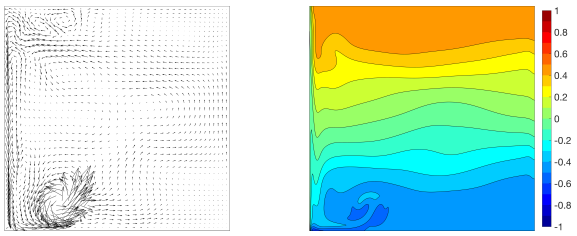

(d) $\tau = 2012.5$ (end of cooling)

Figure 2: Velocity vectors (left) and temperature contours (right) for $Ra = 1 \times 10^8$, $Pr = 0.7$ and $f = 0.08$.

In the first half of the heating phase, shown in figure 2(a), the temperature on the wall rises from $\theta = 0$ to 1. Heat is transferred from the wall to the near-wall region by conduction, forming a positively buoyant NCBL that is beginning to discharge into a small intrusion at the top left corner. A clockwise circulation, associated with the rising boundary layer, is seen adjacent to the heated wall, while an anti-clockwise circulation, generated

in the previous cooling cycle, spans most of the rest of the cavity. Meanwhile, a strong but small counter-clockwise circulation is observed near the bottom wall, centered at approximately a quarter of the cavity width from the left sidewall, which is a remnant of the cold intrusion in the previous cooling phase. At the end of the heating phase (figure 2(b)), the rising boundary layer discharges into a distinct hot intrusion, spanning approximately 30% of the cavity width. The clockwise circulation, which is now located at the head of the intrusion, one quarter of the way across the cavity immediately below the upper boundary, becomes more intense. The counter-clockwise circulation near the bottom loses its strength, and the remnant cold intrusion completely breaks up and merges into the existing cold region. When the cooling phase starts, the cold temperature on the wall produces a negatively buoyant falling NCBL, in figure 2(c), the hot intrusion detaches from the boundary layer, and breaks up into a similar shape as the cold intrusion remnant in figure 2(a) at maximum heating. The falling boundary layer has an associated counter-clockwise circulation, which moves down to the bottom left corner and merges into the existing counter-clockwise circulation at the end of the cooling phase in figure 2(d). The central region of the cavity is strongly stratified throughout the cycle.

The overall stratification parameter S is used to quantify the thermal structure of the flow, where

$$S = \iint_{\Omega} \frac{\partial \theta}{\partial y} d\Omega. \tag{12}$$

Figure 3 shows the time series of S together with the corresponding fast Fourier transform (FFT) for the $f = 0.08$ case described above. The sampling frequency is 2000, and the power of the FFT is scaled by the length of the signal. M is the modal frequency of S normalised by the forcing frequency, f.

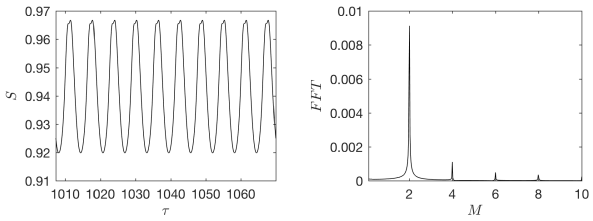

Figure 3: Stratification time series (left) and fast Fourier transform (right) for $Ra = 1 \times 10^8$, $Pr = 0.7$ and $f = 0.08$.

Three key quantities may be obtained from the time series and FFT, the structure of the response frequencies of S, the stratification strength, $\overline{S}$, given by the mean value of S at full development, and the amplitude of the fluctuations, $A(S)$, obtained as the difference between the maximum and minimum values of S at full development. The FFT result reveals that the dominant mode is $M = 2$, corresponding to two times the forcing frequency, with three super-harmonic modes visible, $M = 4$, 6, and 8. The strength of stratification is $\overline{S} = 0.9417$ and the amplitude is $A(S) = 0.0469$.

The time series of S and the FFT results for forcing frequency, $f = 0.125$, are shown in figure 4. The flow is displaying a different behaviour at this frequency, compared to the lower frequency above, with additional lower frequency modes evident in this time series, rather than the single mode appearance at $f = 0.08$. FFT analysis reveals that multiple sub-harmonic modes are excited, more significantly at $M = 0.25$, 0.5 and 1. Additionally, around the dominant and super-harmonic modes, two weak subsidiary modes are triggered symmetrically at $M = 2 \pm 0.5$, 4 ± 0.5 and 6 ± 0.5.

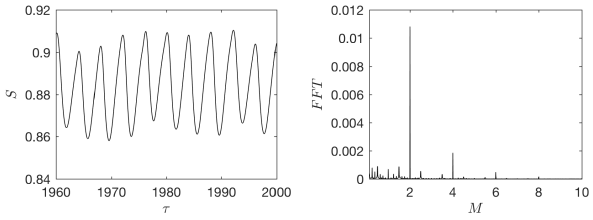

Figure 4: Stratification time series (left) and fast Fourier transform (right) for $Ra = 1 \times 10^8$, $Pr = 0.7$ and $f = 0.125$.

FFT results for additional frequencies are shown in figure 5, again for $Ra = 1 \times 10^8$, $Pr = 0.7$. In all cases, the dominant mode is $M = 2$. Super-harmonic modes are observed for all cases, although they are very weak at the highest frequency $f = 2$. Sub-harmonic modes are noticeably observed only for $0.1 \leqslant f \leqslant 0.15$. The appearance of sub-harmonic modes and the large super-harmonics suggest the occurrence of resonance for the range of forcing frequencies $0.1 \leqslant f \leqslant 0.15$.

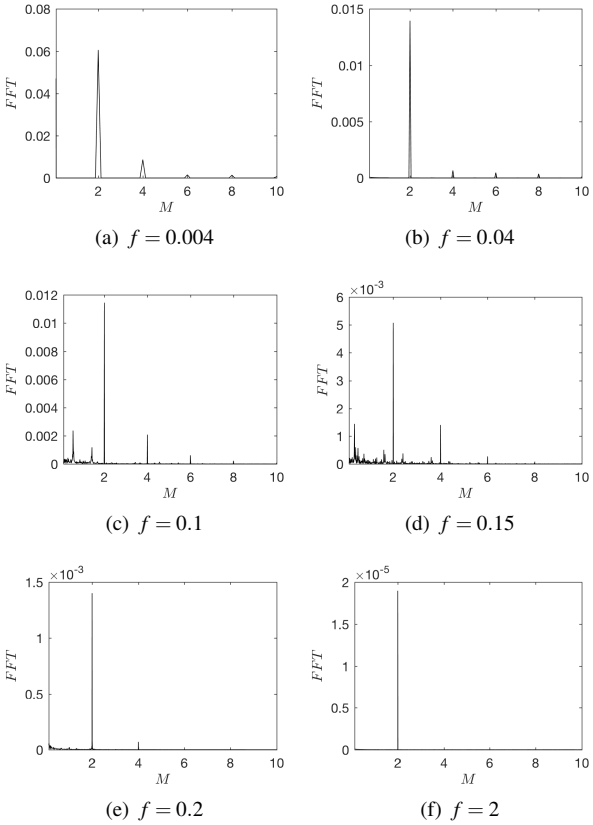

(a) $f = 0.004$ (b) $f = 0.04$

(c) $f = 0.1$ (d) $f = 0.15$

(e) $f = 0.2$ (f) $f = 2$

Figure 5: Fast Fourier transform of stratification time series for $Ra = 1 \times 10^8$, $Pr = 0.7$ with various forcing frequencies.

The time averaged stratification $\overline{S}$ and the stratification perturbation amplitude $A(S)$ are plotted against f in figure 6. The strength of the stratification increases with the forcing frequency up to $f \cong 0.008$, has little variation in the range $0.008 \lessapprox f \lessapprox 0.1$, and decreases rapidly for $f \gtrapprox 0.2$. In the range of forcing frequency $0.1 \leqslant f \leqslant 0.15$, $\overline{S}$ has an evident local amplification in values, supporting the observations of the FFT results that the flow is exhibiting resonance in this range. Similar resonance effects are also observed in the plot of amplitude against forcing frequency in figure 6(b).

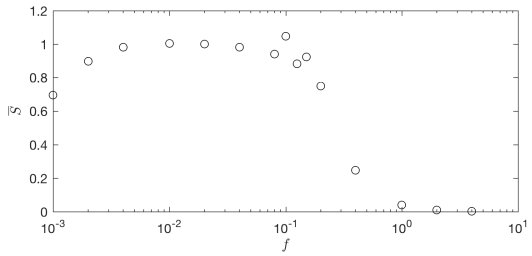

(a) Stratification strength

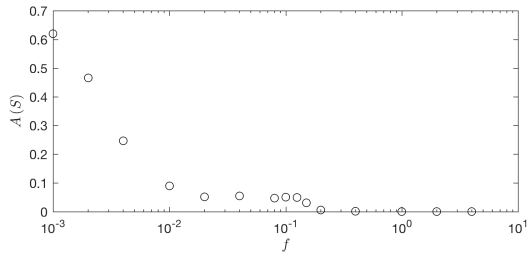

(b) Stratification amplitude

Figure 6: Stratification strength and amplitude for $Ra = 1 \times 10^8$, $Pr = 0.7$ ($0.001 \leq f \leq 10$).

As noted above, it is believed that the resonance is a result of the interaction of the forcing frequency with internal waves. The fundamental mode of internal wave oscillations, written using $\overline{S}$ as the stratification parameter in the present non-dimensional form, is

$$f_i = \frac{1}{2\pi} \frac{\overline{S}}{\sqrt{2} Pr^{\frac{1}{2}}}. \tag{13}$$

Figure 7 contains the mode one frequency f_i plotted against forcing frequency, with the dashed line equal to f. The forcing frequency for $f_i \cong f$, i.e. f at the intersection point, is in the suggested resonance range $0.1 \leqslant f \leqslant 0.15$, indicating the fundamental mode internal wave may be excited, leading to the observed effects.

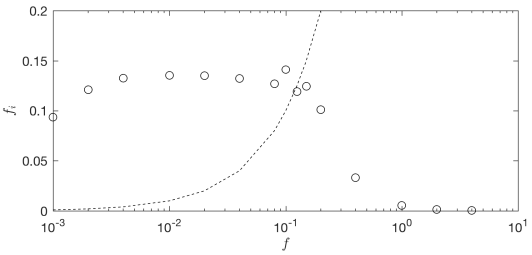

Figure 7: First mode frequency of internal waves for $Ra = 1 \times 10^8$, $Pr = 0.7$ ($0.001 \leq f \leq 10$).

Conclusion

Numerical simulations are carried out for natural convection flow in an air-filled cavity subjected to periodic heating/cooling of one wall. The periodic thermal forcing produces an alternating-direction NCBL that discharges flow into a hot/cold intrusion near the top/bottom of the cavity. The flow is stably stratified in the interior, and the stratification parameter varies with time. The dominant stratification response frequency is twice the forcing frequency, while the stratification strength and amplitude are strongly dependent on the forcing frequency.

Resonance like effects are observed for $Ra = 1 \times 10^8$, $Pr = 0.7$ at $f \cong 0.125$. At this frequency, the stratification time series has sub-harmonic modes, together with amplified dominant and super-harmonic modes. Local amplifications of the stratification amplitude and strength are also observed in the proposed resonance range. The first mode of the internal wave oscillation is calculated for the present case and is found to be very close to the forcing frequency at $f \cong 0.125$, supporting the hypothesis that the observed behaviour may be a result of the resonant interaction of the forcing mode and the internal wave mode.

Acknowledgements

The authors acknowledge the support of the Australian Research Council.

References

[1] Catton, I., Natural convection in enclosures, in *Proceedings of the sixth international heat transfer conference*, 1978, volume 6, 13–31.

[2] Cheikh, N. B., Beya, B. B. and Lili, T., Aspect Ratio Effect on Natural Convection Flow in a Cavity Submitted to a Periodical Temperature Boundary, *Journal of Heat Transfer*, **129**, 2006, 1060–1068.

[3] Kalabin, E. V., Kanashina, M. V. and Zubkov, P. T., Heat transfer from the cold wall of a square cavity to the hot one by oscillatory natural convection, *Numerical Heat Transfer, Part A: Applications*, **47**, 2005, 609–619.

[4] Kalabin, E. V., Kanashina, M. V. and Zubkov, P. T., Natural-convective heat transfer in a square cavity with time-varying side-wall temperature, *Numerical Heat Transfer, Part A: Applications*, **47**, 2005, 621–631.

[5] Kazmierczak, M. and Chinoda, Z., Buoyancy-driven flow in an enclosure with time periodic boundary conditions, *International Journal of Heat and Mass Transfer*, **35**, 1992, 1507–1518.

[6] Kwak, H. S. and Hyun, J. M., Natural convection in an enclosure having a vertical sidewall with time-varying temperature, *Journal of Fluid Mechanics*, **329**, 1996, 65–88.

[7] Lage, J. L. and Bejan, A., The resonance of natural convection in an enclosure heated periodically from the side, *International Journal of Heat and Mass Transfer*, **36**, 1993, 2027–2038.

[8] Ostrach, S., Natural convection heat transfer in cavities and cells, in *Proceedings of the seventh international heat transfer conference*, 1982, volume 1, 365–379.

[9] Patterson, J. and Imberger, J., Unsteady natural convection in a rectangular cavity, *Journal of Fluid Mechanics*, **100**, 1980, 65–86.

[10] Patterson, J. C. and Armfield, S. W., Transient features of natural convection in a cavity, *Journal of Fluid Mechanics*, **219**, 1990, 469–497.

[11] Zhou, L. and Armfield, S., A compact fourth-order spatial discretisation applied to the Navier-Stokes equations, *ANZIAM Journal*, **56**, 2016, 481–501.

[12] Zhou, L., Armfield, S. W., Williamson, N., Kirkpatrick, M. P. and Lin, W., Transient natural convection flow in a cavity subject to time-varying sidewall heating and cooling, in *Proceedings of the 20th Australasian Fluid Mechanics Conference*, Perth, WA, Australia, 2016.